Calorimetric study of the nematic to smectic-*A* and smectic-*A* to smectic-*C* phase transitions in liquid-crystal–aerosil dispersions

A. Roshi and G. S. Iannacchione*
Department of Physics, Worcester Polytechnic Institute, Worcester, Massachusetts 01609, USA

P. S. Clegg
Department of Physics and Astronomy, University of Edinburgh, Edinburgh EH9 3JZ, United Kingdom

R. J. Birgeneau
Department of Physics, University of California, Berkeley, California, 94720, USA

M. E. Neubert
Liquid Crystal Institute, Kent State University, Kent, Ohio 44242, USA
(Received 10 May 2005; published 23 November 2005)

A high-resolution calorimetric study has been carried out on nanocolloidal dispersions of aerosils in the liquid crystal 4-*n*-pentylphenylthiol-4′-*n*-octyloxybenzoate ($\bar{8}$S5) as a function of aerosil concentration and temperature spanning the smectic-*C* to nematic phases. Over this temperature range, this liquid crystal possesses two continuous *XY* phase transitions: a fluctuation-dominated nematic to smectic-*A* transition with $\alpha \approx \alpha_{XY}=-0.013$ and a mean-field smectic-*A* to smectic-*C* transition. The effective critical character of the *N*-Sm*A* transition remains unchanged over the entire range of the introduced quenched random disorder while the peak height and enthalpy can be well described by considering a cutoff length scale to the quasicritical fluctuations. The robust nature of the *N*-Sm*A* transition in this system contrasts with cyanobiphenyl-aerosil systems and may be due to the mesogens being nonpolar and having a long nematic range. The character of the Sm*A*-Sm*C* transition changes gradually with increasing disorder but remains mean field like. The heat capacity maximum at the Sm*A*-Sm*C* transition scales as $\rho_S^{-0.5}$ with an apparent evolution from tricritical to a simple mean-field step behavior. These results may be generally understood as a stiffening of the liquid crystal (both the nematic elasticity as well as the smectic layer compression modulus *B*) with silica density.

DOI: 10.1103/PhysRevE.72.051716 PACS number(s): 64.70.Md, 61.30.Eb, 65.40.Ba

I. INTRODUCTION

The study of quenched random disorder effects addresses many fundamental issues of current interest in statistical mechanics. Recent experimental advances have shed considerable light on the random-field-theoretic approach, believed to be underlying the physics of quenched random disorder (QRD). In particular, these efforts have led to the systematic study of the random-field model for transitions that break a continuous symmetry [1]. This model is applicable to a terrific range of phenomena: These include unique assemblies of colloids, complex fluids, charge density waves, spin glasses, and doped semiconductors, to name a few. The experimental efforts to date have focused on idealized physical systems in order to isolate the essential features of quenched random disorder. Considerable research has been carried out on the superfluid transition of ^{4}He and ^{4}He-^{3}He mixtures in a variety of porous media [2,3] as well as doped magnetic systems [4] but many questions remain due to the quantum nature of the former and the glasslike behavior of the latter [1].

In the random-field approach, the effect of the disorder is mapped onto a local field $\vec{h}(\vec{r})$ directly coupled to the order parameter. This local field varies randomly through the system on length scales smaller than the length scales of the ordered phase such that $\langle \vec{h} \rangle_{\vec{r}} = \vec{0}$ while $\langle \vec{h} \cdot \vec{h} \rangle_{\vec{r}} \neq 0$. Because the nature of the imposed disorder is modeled as a dilute (or weak) random field, the effect of QRD may be understood statistically. By studying in detail good realizations of particular universality classes, the results can be applied more generally to a wide variety of physical systems. A particularly fruitful physical system to explore QRD effects in general and the random-field model in particular has been nanocolloidal dispersions of an aerosil gel in a liquid-crystal (LC) host (LC+sil) [1,5].

The most well-studied LC+sil phase transition has been the continuous nematic to smectic-*A* (*N*-Sm*A*) phase transition. This transition involves the breaking of a continuous symmetry and belongs, though not simply, to the three-dimensional (3D) *XY* universality class [6]. In general, high-resolution x-ray [7–10] and calorimetry [5,11–15] studies of the *N*-Sm*A*+sil transition have found that the (quasi-)long-range-ordered smectic phase is destroyed for all densities of aerosil. However, below a silica density of about 0.1 g of SiO_2 per cm^3 of LC (the so-called conjugate density ρ_S [1], whose units will be dropped hereafter), a pseudotransition displaying quasicritical behavior at $T=T^*$ persists. The scattering from the short-range smectic order is well described by both a bulk thermal structure factor (dominate above the

*Electronic address: gsiannac@wpi.edu

pseudotransition T^*) and a random-field structure factor (dominate below T^*) given by the bulk thermal form squared, the so-called "Lorentzian+Lorentzian-squared" form [7,8]. Although the smectic correlation length is finite, it is large (spanning many mean-void lengths of the silica gel) and exhibits a power-law divergence on cooling to T^* at which it saturates for 8CB [7] and 8OCB [9] in aerosils or begins to decrease upon further cooling towards the Sm*C* phase for $\bar{8}$S5+sil system [10]. This broadening observed for $\bar{8}$S5 +sil [10] and anisotropic (field aligned) $\bar{8}$S5+sil [16] samples could be due to a distribution of Sm*C* tilt angles and result in a lower average order parameter squared. The calorimetry studies found sharp, quasicritical, power-law divergences for the heat capacity for $\rho_S < 0.1$, while all phase transitions appear to be elastically smeared for larger ρ_S [1]. The evolution of an effective critical heat-capacity exponent α_{eff} with aerosil density is consistent with a gradual drop in the nematic susceptibility with increasing gel density for all *N*-Sm*A* transitions studied to date.

A detailed scaling analysis of the *N*-Sm*A* transition combining x-ray and calorimetry results through the quasicritical transition for low aerosil density revealed the importance of both random-field and finite-size-like effects [8,17]. The dimensionality of the system also played a role and was consistent with the expected dimensional rise, $d_{rf}=d+2$, for a system with random-field disorder [18,19]. This work also found in general that the effective random-field strength (or variance) scales as ρ_S over the entire range of silica densities studied thus far, although there are indications of different scalings above and below $\rho_S=0.1$ [17]. The experimental and theoretical results to date support the view that a random-field–*XY* (RF-*XY*) system has no new critical point.

Recently, tilted smectic phases have become the focus of studies on quenched random disorder effects [10,5]. The smectic-*A* to smectic-*C* (Sm*A*-Sm*C*) phase transition involves the breaking of a continuous symmetry and is described by two parameters, the tilt and azimuthal angles. This transition belongs to the 3D *XY* universality class but is mean field in character due to the relatively long bare correlation length of the Sm*C*. The strong coupling between tilt and smectic layer compression for the Sm*C* phase appears to place the Sm*A*-Sm*C* transition always close to a (Landau) mean-field tricritical point [6]. A consequence of the tilt angle's sensitivity to the layer elasticity is that this transition is much more strongly disordered by perturbations that distort the smectic layers, as in the strong disorder of aerogels, than the *N*-Sm*A* [20,21]. For weaker aerosil-gel-induced disorder, the Landau mean-field heat-capacity signature was found to be unaffected by hydrophobic aerosils [12] while a recent high-resolution x-ray scattering study on a different LC in a hydrophilic aerosil found little change in the tilt-angle temperature dependence with ρ_S [10]. This robustness to weak disorder may be a consequence of the mean-field character of the transition, placing it effectively at its upper critical dimension. However, when the transition from the Sm*A* phase goes to the chiral analog of the Sm*C* phase (SmC^*), the effect of even the aerosil-induced disorder generally suppresses and smears the transition [5].

The present work focuses on the effect of quenched random disorder induced by a nanocolloidal dispersion of hydrophilic type-300 aerosil forming a mass-fractal gel within the liquid crystal 4-*n*-pentylphenylthiol-4′-*n*-octyloxybenzoate ($\bar{8}$S5) that closely follows the previously reported x-ray studies [10]. High-resolution calorimetry has been carried out on these $\bar{8}$S5+sil dispersions as a function of aerosil concentration and temperature spanning the smectic-*C* to nematic phases. This liquid crystal possesses two continuous *XY* phase transitions of interest. The first is a fluctuation-dominated nematic to smectic-*A* characterized by a heat capacity exponent $\alpha \lesssim 0$. The critical character of the *N*-Sm*A* transition remains unchanged with the introduction of the quenched random disorder while its enthalpy and heat-capacity maximum decrease in a manner consistent with a finite-size-like scaling without any obvious crossover from soft to stiff gel seen on other LC+sil systems. The stability of the heat capacity quasicritical behavior for this system with QRD is consistent with our understanding of the influence of the gel on the underlying nematic order. Since in the bulk material the nematic susceptibility is low before Sm*A* order begins to form, the gel has little scope to reduce this quantity.

The second is a mean-field Landau tricritical smectic-*A* to smectic-*C* phase transition. The Sm*A*-Sm*C* remains mean field for all aerosil concentrations studied with an continuous evolution from the bulk's tricritical to a simple mean-field step heat-capacity behavior analogous to that seen for the pure Sm*A*-SmC^* transition in binary LC mixtures [22]. In particular, the Sm*A*-Sm*C* heat capacity maximum at the transition scales as $\rho_S^{-0.5}$. The stable mean-field character of the Sm*A*-Sm*C* with QRD may be a consequence of this transition being effectively, due to the long-range interactions, at its upper critical dimension. The observed crossover from tricritical to a simple mean-field step behavior for the Sm*A*-Sm*C* and the continuous diminishing of the *N*-Sm*A* heat capacity peaks may be understood as a continuous stiffening of the liquid-crystal elasticity for the nematic and smectic structure with increasing silica density. However, many theoretical challenges are evident.

Section II describes the preparation of the $\bar{8}$S5+sil dispersions as well as the ac-calorimetry technique employed. Section III presents the results of the calorimetric study, while Sec. IV discusses the significance of the evolution of an *XY* transition as well as a crossover from Landau tricritical to mean-field continuous transition with increasing quenched disorder. Directions for future study will also be discussed.

II. SAMPLES AND CALORIMETRY

The liquid crystal $\bar{8}$S5, synthesized at Kent State University, was used after degassing in the isotropic phase for 2 h. The best literature-reported transition temperature values in the bulk for this liquid-crystal molecule (M_w =412.64 g mol^{-1}) are $T^0_{IN} \cong 359.6$ K for the weakly first-order isotropic to nematic (*I*-*N*) transition, $T^0_{NA} \cong 336.58$ K for the *XY*-like continuous nematic to smectic-*A* (*N*-Sm*A*) transition, and $T^0_{AC} \cong 329.35$ K for the monotropic Landau tricritical smectic-*A* to smectic-*C* (Sm*A*-Sm*C*) transition [23]. At lower temperatures on cooling, a monotropic

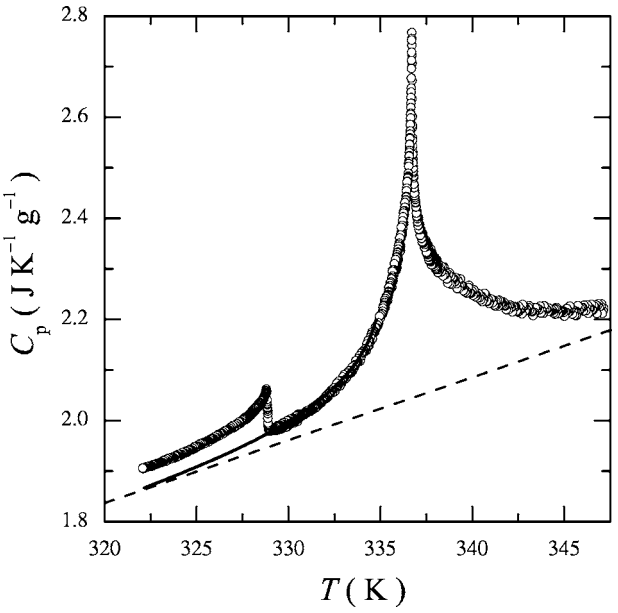

FIG. 1. The specific heat of bulk $\bar{8}$S5 on cooling spanning the nematic, smectic-*A*, and smectic-*C* phases. The dashed line represents the linear C_p (background) used to extract the excess C_p associated with the *N*-Sm*A* transition, $\Delta C_p(NA)$. The solid line represents the low-temperature wing of the *N*-Sm*A* transition and is used to extract the excess C_p associated with the Sm*A*-Sm*C* transition, $\delta C_p(AC)$.

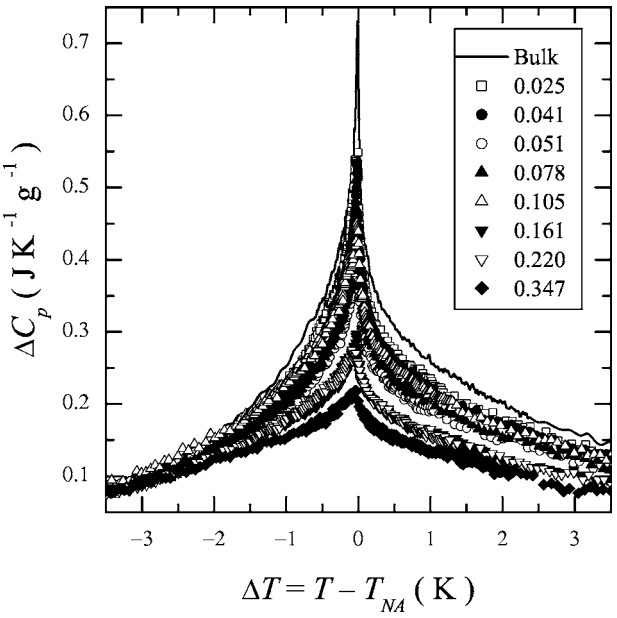

FIG. 2. Excess specific heat ΔC_p of the *N*-Sm*A* transition ±3.5 K about T_{NA} for bulk $\bar{8}$S5 and $\bar{8}$S5+sil samples. The inset lists the ρ_S for each data set shown. The temperature range shown corresponds approximately to $\pm 10^{-2}$ width in reduced temperature.

smectic-*C* to crystal-*B* (Sm*C*-Cr*B*) transition occurs at $T^0_{CB} \sim 304$ K. The strongly first-order Crystal-Sm*A* (Cr-Sm*A*) transition occurs reproducibly on heating at $T^0_{CrA} \sim 332$ K. The measured transitions temperatures for our bulk material occur at $T^0_{NA} \cong 336.64$ K, $T^0_{AC} \cong 328.96$ K, and $T^0_{CrA} \sim 331.0$ K, which are in reasonable agreement with the literature bulk values. However, $\bar{8}$S5 is known to age with its transition temperatures continuously shift downward with time, especially when heated into the isotropic phase [23,24]. Fortunately, the *N*-Sm*A* and Sm*A*-Sm*C* transitions remain relatively sharp, well defined, and consistent in shape during the sample aging; see Figs. 1 and 2 as well as Table I. Although the aging of this LC is unavoidable, the samples studied in this work all experienced the same preparation method and thermal history; thus, the relative evolution of these transitions with aerosil disorder should be preserved.

The nanocolloidal mixture of hydrophilic type-300 aerosil in $\bar{8}$S5 was prepared following the solvent dispersion procedure outlined in Refs. [9,10]. The hydrophilic nature of the aerosils allows the silica particles to weakly hydrogen bond to each other and form a gel in an organic solvent. The specific surface area of type-300 aerosil is 300 m^2 g^{-1} [25], and each aerosil sphere is roughly 7 nm in diameter. However, the basic free-floating aerosil unit consists of a few of these spheres fused together during the manufacturing process [14]. Each $\bar{8}$S5+sil sample was created by mixing appropriate quantities of liquid crystal and aerosil together, then dissolving the resulting mixture in spectroscopic-grade (low-water-content) acetone. The resulting solution was then dispersed using an ultrasonic bath for about an hour. As the acetone evaporates from the mixture, a fractal-like gel forms through diffusion-limited aggregation. Crystallization of the LC host can severely disrupt the gel structure, and so care was taken to prevent any formation of the solid phase of the liquid crystal during the experiments.

High-resolution ac calorimetry was performed using two homebuilt calorimeters at WPI. The sample cell consisted of a silver crimped-sealed envelope ~10 mm long, ~5 mm wide, and ~0.5 mm thick (closely matching the dimensions of the heater). After the sample was introduced into a cell having an attached 120-Ω strain-gauge heater and 1-MΩ carbon-flake thermistor, a constant current was placed across the heater to maintain the cell temperature well above T_{IN}. The filled cell was then placed in an ultrasonic bath to remix the sample. After remixing, the cell was mounted in the calorimeter, the details of which have been described elsewhere [26]. In the ac mode power is input to the cell as $P_{ac}e^{i\omega t}$, resulting in temperature oscillations with amplitude T_{ac} and a relative phase shift of $\varphi \equiv \Phi + \pi/2$, where Φ is the absolute phase shift between $T_{ac}(\omega)$ and the input power. The specific heat at a heating frequency ω using $C^* \equiv P_{ac}/\omega|T_{ac}|$ is given by

$$C_p = \frac{[C'_{filled} - C_{empty}]}{m_{sample}} = \frac{C^* \cos\varphi - C_{empty}}{m_{sample}}, \tag{1}$$

$$C''_{filled} = C^* \sin\varphi - \frac{1}{\omega R_e}, \tag{2}$$

where C'_{filled} and C''_{filled} are the real and imaginary components of the heat capacity, C_{empty} is the heat capacity of the cell and silica, m_{sample} is the mass in grams of the liquid crystal (the total mass of the $\bar{8}$S5+sil sample was ~20 mg,

TABLE I. Summary of the calorimetric results for $\bar{8}$S5+sil samples. Shown are the conjugate silica density (ρ_S in grams of aerosil per cm^3 of $\bar{8}$S5), the mean-void length $l_0=2/a\rho_S$ (where $a=300$ m^2 g^{-1} is the specific surface area of this aerosil) within the gel in Å, the *N*-Sm*A* (T_{NA}) and the Sm*A*-Sm*C* (T_{AC}) pseudophase transition temperatures, and the smectic-*A* temperature range ($\Delta T_A=T_{NA}-T_{AC}$) all in kelvins and averaged between heating and cooling scans. These are followed by similarly averaged enthalpy (δH_{NA}) in J g^{-1} and specific heat maximum $h_m \equiv \Delta C_p^{max}$ in J K^{-1} g^{-1} values for the *N*-Sm*A* pseudophase transition. The final column tabulates the specific heat step in J K^{-1} g^{-1} of the Sm*A*-Sm*C* phase transition δC_{AC}^{Step} averaged between heating and cooling scans and taken as the value of the excess specific heat −6 K below T_{AC}.

ρ_S	l_0	T_{NA}	T_{AC}	ΔT_A	δH_{NA}	h_m	δC_{AC}^{Step}
0	∞	336.626	329.009	7.617	2.136	0.726	0.044
0.025	2636	336.073	328.836	7.237	1.985	0.541	0.043
0.041	1636	336.524	329.136	7.388	1.897	0.530	0.034
0.051	1303	336.315	329.124	7.191	1.780	0.377	0.025
0.078	859	336.519	329.527	6.992	1.834	0.487	0.032
0.105	636	336.676	329.210	7.466	1.952	0.444	0.027
0.161	414	336.573	329.456	7.117	1.573	0.302	0.014
0.220	303	336.865	329.915	6.950	1.561	0.284	0.013
0.347	192	336.505	329.621	6.884	1.404	0.231	0.003

which yielded m_{sample} values in the range of 13–20 mg), and R_e is the external thermal resistance linking the cell and the bath (here, ~200 K W^{-1}). Equations (1) and (2) require a small correction to account for the finite internal thermal resistance compared to R, and this was applied to all samples studied here [27]. Measurements were conducted at various frequencies from 1 to 500 mHz in order to ensure the applicability of Eqs. (1) and (2). For all results presented here, $C''_{filled} \simeq 0$ through the *N*-Sm*A* and Sm*A*-Sm*C* transitions, which is expected for continuous phase transitions, and C_p was independent of ω. All data presented here were taken at a heating frequency of $\omega=0.1473$ s^{-1} (or 23.4 mHz) and a scanning rate of less than ±100 mK h^{-1}, which yielded static C_p results. This equilibrium behavior relates only to the pseudocritical smectic fluctuations that are the focus of this work. The glasslike behavior, which has been observed in rheological studies in this frequency range [35], is a characteristic of these systems away from the pseudotransition.

The bulk $\bar{8}$S5 and all $\bar{8}$S5+sil samples experienced the same thermal history after mounting, 6 h in the isotropic phase to ensure homogeneous gelation, then a slow cool into the smectic phase at ~320 K before beginning the first detailed heating scan to ~345 K followed immediately by a detailed cooling scan over the same range. Tests on bulk $\bar{8}$S5 with various thermal histories in the isotropic phase reveal an aging of the material. There are progressive shifts of the transition temperatures downward with increased time at high temperature. However, other than an increase in the rounding of the C_p peaks and the downward shift of the transition with time, the critical character remains essentially unchanged.

III. RESULTS

The specific heat on cooling for a bulk sample of $\bar{8}$S5 is shown in Fig. 1. Clearly visible are the *XY*-like *N*-Sm*A* phase transition at 336.71 K and a Landau mean-field Sm*A*-Sm*C* at 328.82 K. These are in good agreement with Schantz and Johnson [23]. The excess specific heat due to the *N*-Sm*A* transition $\Delta C_p(NA)$ for the bulk and LC+sil samples is obtained by subtracting from the specific heat C_p a linear background:

$$\Delta C_p = C_p - C_p \text{ (background)}, \tag{3}$$

where C_p (background) is shown as the dashed line in Fig. 1 and represents the C_p variation of the low-temperature *wing* of the *I*-*N* transition. This expression is a valid representation of $\Delta C_p(NA)$ for all $T > T_{AC}$ and the resulting $\Delta C_p(NA)$ for all samples studied are shown in Fig. 2 over a ±3.5 K temperature range about T_{NA}. The fluctuation dominated *N*-Sm*A* transition enthalpy is defined as

$$\delta H_{NA} = \int \Delta C_p(NA) dT, \tag{4}$$

where consistent limits of the integration of ±5 K about T_{NA} were used for all samples. The specific heat contribution of the Sm*A*-Sm*C* transition is obtained from ΔC_p by subtracting the low-temperature heat capacity *wing* of the *N*-Sm*A* transition (see Fig. 1):

$$\delta C_p(AC) = \Delta C_p - \Delta C_p^{wing}(NA). \tag{5}$$

The result for all samples studied are shown in Fig. 3 over a range +2 K above to −4.5 K below T_{AC}. The relevant thermal characteristics for both phase transitions of $\bar{8}$S5+sils as a function of ρ_S are given in Table I.

As seen in Fig. 2, the *N*-Sm*A* C_p peak remains sharp for all aerosil densities up to the maximum studied of $\rho_S=0.347$ with no abrupt truncation marking a transition from soft to stiff gel behavior seen in 8CB+sil [14] and 8OCB+sil [28] systems. The $\Delta C_p(NA)$ wings on both sides of the transition decrease with increasing ρ_S in contrast with that

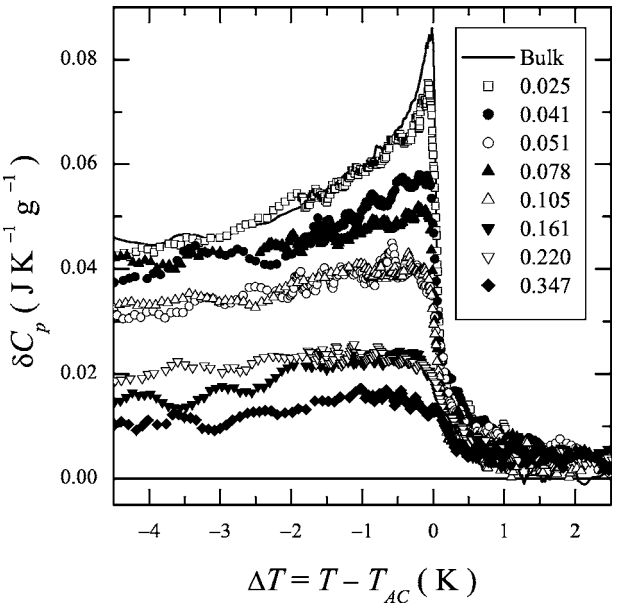

FIG. 3. Excess specific heat δC_p of the SmA-SmC phase transition from +2.5 K above to −4.5 K below T_{AC} for bulk $\bar{8}$S5 and $\bar{8}$S5+sil samples. The inset lists the ρ_S for each data set shown.

found for the 8CB and 8OCB in aerosils, which found significant reduction of the high-temperature $\Delta C_p(NA)$ wing [14]. Qualitatively, the $\Delta C_p(NA)$ peak shape remains remarkably stable with increasing ρ_S. For the $\bar{8}$S5+sil system, the most striking effect of the aerosils is the strong decrease in the heat capacity maximum at the transition, $h_m = \Delta C_p^{max}(NA)$, and in the transition enthalpy δH_{NA} with increasing ρ_S. In addition, the value of $T_{NA}(\rho_S)$ also displays very little sensitivity to the aerosils even when the aging of the $\bar{8}$S5 is taken into account, in stark contrast to the nonmonotonic downward shifts found for nearly all other LC +sil systems [14]. See Table I.

The effect of increasing aerosil concentration on the SmA-SmC transition heat capacity appears entirely at and below the transition T_{AC}. The $\delta C_p(AC)$ peak smoothly evolves with increasing ρ_S from the bulk tricritical behavior to a simple heat capacity step as shown in Fig. 3. Also apparent is the systematic reduction of the step magnitude with increasing ρ_S as listed in Table I. While there is some rounding of $\delta C_p(AC)$ in the immediate vicinity of T_{AC}, there does not appear any strong effect of the aerosil on the high-temperature δC_p tail. As with the N-SmA transition, even when aging of the bulk material is taken into account, $T_{AC}(\rho_S)$ is not shifted downward with increasing aerosil content but appears to shift slightly upward. The stability of both $T_{NA}(\rho_S)$ and $T_{AC}(\rho_S)$ reported here is in contrast to that found in the recent x-ray study that found large nonmonotonic transition temperature shifts with ρ_S [10]. However, the thermal history experienced by these calorimetry samples was far less severe than that experienced by the x-ray samples which were held at high temperatures while the solvent evaporated prior to the measurements. Thus, the results presented here should reflect a consistent measure of the transition temperature shift with ρ_S for this system.

A. *XY*-like *N*-Sm*A* scaling analysis

The shape of these experimental $\Delta C_p(NA)$ data as a function of aerosil content is characterized by a power-law form [29] in terms of the reduced temperature $t = |T - T^*|/T^*$ given by

$$\Delta C_p(NA) = A^{\pm} t^{-\alpha}(1 + D^{\pm} t^{\Delta_1}) + B_c, \tag{6}$$

where the critical behavior as a function of reduced temperature t is characterized by an exponent α, amplitudes $A^{\pm}$ above and below the transition, a critical background term B_c, and corrections-to-scaling terms having an amplitude $D^{\pm}$ and exponent $\Delta_1 \simeq 0.5$. An increasing temperature gap of excluded data about the $\Delta C_p(NA)$ peak with increasing ρ_S was required to perform the nonlinear least-squares fitting. These excluded data were identified by strong deviations in the residuals near T^* and represent rounded $\Delta C_P(NA)$ values not describable by the power law given in Eq. (6). These fit results for the sets of heating and cooling scans of bulk $\bar{8}$S5 and $\bar{8}$S5+sil samples are presented in Tables II and III, respectively. In addition to fits with the effective critical exponent α_{eff} as a free parameter, fits were also performed with α_{eff} fixed to the 3D XY value of $\alpha_{XY} = -0.013$. The bulk $\bar{8}$S5 fit results are of good quality for both heating and cooling and yield a very small negative α_{eff} that is not significantly different from fixing α_{eff} to $\alpha_{XY} = -0.013$ as indicated by χ_ν^2 [30]. This indicates that the specific heat of the N-SmA transition for the bulk LC behaves essentially as a clean XY transition consistent with the literature [23,31]. However, it should be noted that the critical exponents for the parallel correlation length ($\nu_\parallel$) and for the smectic susceptibility (γ) do not have XY values [29] and that the N-SmA transition for bulk $\bar{8}$S5 exists in a complex crossover regime.

As ρ_S increases for the $\bar{8}$S5+sil samples, the fits for both heating and cooling are all of good quality even up to the highest density studied. In general, the adjustable parameters have approximately a 10% uncertainty in magnitude for the bulk and the two lowest-density aerosil samples, except for T_c which has an uncertainty of approximately ±5 mK for all fits. This uncertainty grows for the higher-density samples because an increasing temperature gap about the ΔC_p peak of data is excluded from the fits due to rounding. These fits show that the critical character described by the exponent α_{eff} of the N-SmA transition remains unchanged in the $\bar{8}$S5 +sil samples for all ρ_S, even above the $\rho_S = 0.1$ where previous studies of other LC+sil samples found no critical behavior [1,14]. It is apparent from the fits that the increasing temperature gap ($\pm t_{min}$) is dominated by rounding on the low-temperature side of the $\delta C_p(NA)$ peak. This increasing temperature gap for the fits has the effect of causing the increase in the magnitudes of the correction-to-scaling coefficients $D^{\pm}$ although they remain well behaved. Fixing the ratio $D^+/D^- = 1$ or setting $D^+ = D^- = 0$ resulted in significantly poorer fits for all samples. It is also evident is that the critical

TABLE II. Heating scan summary of the results of fitting Eq. (6) to the excess specific-heat peak ΔC_p of the *N*-Sm*A* phase transition on $\bar{8}$S5+sil samples. The transition temperature T_C is given in kelvins, while the parameters B_C and $A^{\pm}$ are given in J K^{-1} g^{-1}. The parameters $D^{\pm}$ are dimensionless. All scans were fit from $t_{max}=10^{-2}$ to $\pm t_{min}$. All parameters were free to vary in the fit except when the exponent was fixed to $\alpha_{XY}=-0.013$ (denoted by the square brackets).

ρ_S	T_C	α_{eff}	B_C	A^+	A^-	D^+	D^-	$t_{min}\times 10^{-5}$	χ^2_ν
0	335.220	-7×10^{-5}	1023.600	−1023.760	−1023.630	0.0002	0.0022	+1.80/−12.3	1.266
	335.222	[−0.013]	6.053	−6.260	−6.122	0.0026	0.3712		1.319
0.025	334.712	-1×10^{-4}	536.893	−536.971	−536.845	0.0007	0.0045	+3.50/−29.9	1.073
	334.711	−0.013	4.757	−4.880	−4.741	0.0450	0.5234		1.027
0.041	335.111	-1×10^{-4}	383.615	−383.643	−383.536	0.0016	0.0060	+2.56/−14.2	1.287
	335.110	[−0.013]	4.124	−4.194	−4.076	0.1117	0.5715		1.307
0.051	334.938	-2×10^{-4}	154.089	−154.083	−154.025	0.0045	0.0086	+11.4/−49.2	1.134
	334.937	[−0.013]	3.228	−3.249	−3.186	0.1954	0.4153		1.137
0.078	335.123	-1×10^{-4}	376.628	−376.688	−376.614	0.0010	0.0036	+3.08/−14.9	1.163
	335.123	[−0.013]	4.049	−4.146	−4.064	0.0628	0.3348		1.183
0.105	335.297	-1×10^{-4}	259.368	−259.267	−259.171	0.0049	0.0095	+3.63/−19.3	1.076
	335.297	[−0.013]	2.767	−2.698	−2.593	0.4513	0.9716		1.084
0.161	335.162	-7×10^{-4}	18.744	−18.608	−18.580	0.0655	0.0615	+5.67/−42.3	1.036
	335.161	[−0.013]	1.335	−1.212	−1.181	1.0162	0.9862		1.037
0.220	335.498	-4×10^{-4}	10.314	−10.099	−10.048	0.1651	0.1875	+3.59/−57.5	1.004
	335.496	[−0.013]	0.630	−0.428	−0.373	3.9745	5.2388		1.004
0.347	335.145	-6×10^{-4}	6.892	−6.724	−6.703	0.1839	0.1400	+0.27/−85.1	1.056
	335.144	[−0.013]	0.573	−0.414	−0.391	3.0646	2.4651		1.056

amplitudes above and below the transition, $A^{\pm}$, systematically decrease with increasing ρ_S although the ratio A^+/A^- remains unchanged.

The scaling analysis for the *N*-Sm*A* transition in LC+aerosil systems follows that of Ref. [17] by using the correlation length power law to equate the cutoff length scale

TABLE III. Cooling scan summary of the results of fitting Eq. (6) to the excess specific-heat peak ΔC_p of the *N*-Sm*A* phase transition on $\bar{8}$S5+sil samples. The labels are the same as those used in Table II as well as the uncertainties of the adjustable fit parameters.

ρ_S	T_C	α_{eff}	B_C	A^+	A^-	D^+	D^-	$t_{min}\times 10^{-5}$	χ^2_ν
0	335.198	-7×10^{-5}	1047.600	−1047.800	−1047.670	−0.0001	0.0019	+3.42/−9.91	1.463
	335.197	[−0.013]	6.565	−6.826	−6.688	−0.0499	0.2870		1.532
0.025	334.632	-1×10^{-4}	474.449	−474.466	−474.327	0.0012	0.0060	+7.86/−32.8	1.159
	334.630	[−0.013]	4.422	−4.484	−4.334	0.0956	0.6721		1.176
0.041	335.108	-3×10^{-4}	141.506	−141.494	−141.395	0.0056	0.0167	+4.37/−23.5	1.203
	335.108	[−0.013]	3.844	−3.868	−3.760	0.1782	0.6412		1.207
0.051	334.845	-1×10^{-4}	216.789	−216.692	−216.619	0.0047	0.0091	+11.0/−36.4	1.134
	334.843	[−0.013]	2.611	−2.541	−2.462	0.3824	0.8130		1.138
0.078	335.057	-2×10^{-4}	195.069	−195.050	−195.018	0.0050	0.0069	+32.6/−32.7	1.188
	335.055	[−0.013]	3.800	−3.809	−3.775	0.2461	0.3545		1.192
0.105	335.179	−0.0043	11.848	−11.888	−11.823	0.0425	0.1152	+37.0/−68.2	1.145
	335.178	[−0.013]	4.239	−4.301	−4.232	0.1061	0.3208		1.145
0.161	335.123	-4×10^{-4}	48.578	−48.455	−48.427	0.0192	0.0211	+16.4/−39.1	1.151
	335.121	[−0.013]	1.647	−1.538	−1.508	0.6025	0.6853		1.152
0.220	335.458	-3×10^{-4}	33.646	−33.468	−33.415	0.0363	0.0481	+19.7/−99.6	1.032
	335.455	[−0.013]	1.205	−1.043	−0.985	1.1714	1.6754		1.032
0.347	335.14	-3×10^{-4}	9.953	−9.734	−9.706	0.1367	0.1229	+5.65/−74.2	1.129
	335.14	[−0.013]	0.332	−0.119	−0.088	11.6406	14.1668		1.129

(maximum correlation length) ξ_M to a minimum reduced temperature. This is closely related to a finite-size effect; however, there are no true pores and the LC-filled voids are highly interconnected. The correlation length is given by

$$\xi_{\|} = \xi_{\|0} t^{-\nu_{\|}}. \tag{7}$$

Since Eq. (7) is defined only for $T > T^*$, the finite-scale-induced rounding of the transition is estimated in terms of the minimum reduced temperature on the high-temperature side of the transition t_m^+, by the form

$$\delta T^*/T^* \approx 2t_m^+ = 2\left(\frac{\xi_M}{\xi_{\|0}}\right)^{-1/\nu_{\|}} = 2\left(\frac{\xi_{\|0}}{2n} a\rho_S\right)^{1/\nu_{\|}}, \tag{8}$$

where the cutoff length scale is written in terms of n, the number of mean-void lengths l_0. The heat capacity maximum at the transition h_m is given by substituting t_m^+ into Eq. (3) and is also explicitly defined for the $T > T^*$. The explicit form for h_m is

$$h_m = A^+\left(\frac{\xi_M}{\xi_{\|0}}\right)^{\alpha/\nu_{\|}}\left(1 + D^+\left(\frac{\xi_M}{\xi_{\|0}}\right)^{-\Delta_1/\nu_{\|}}\right) + B_c. \tag{9}$$

Finally, the transition enthalpy δH_{NA} resulting from this scaling analysis is determined by using t_m^+ to truncate the integration of Eq. (3) both above and below the transition T^*.

Plotted in Fig. 4 are the scaling trends for the N-SmA transition of $\bar{8}$S5+sil samples using the *bulk* N-SmA $\bar{8}$S5 critical parameters. Two choices for the cutoff length scale are shown. The first choice for the cutoff correlation length ξ_M uses the mean distance between silica surfaces (mean void size), $l_0 = 2/a\rho_S$, where a is the specific surface area [1]. The second choice allows ξ_M to vary as some multiple of l_0—i.e., $\xi_M = nl_0$. The results for h_m of the $\bar{8}$S5+sil samples are in very good agreement using $\xi_M \equiv 3l_0$, which more closely matches the measured saturated smectic correlation length [10]. However, $\delta T^*/T^*$ appears *sharper* and δH_{NA} *smaller* for $\rho_S > 0.1$ than predicted by this analysis.

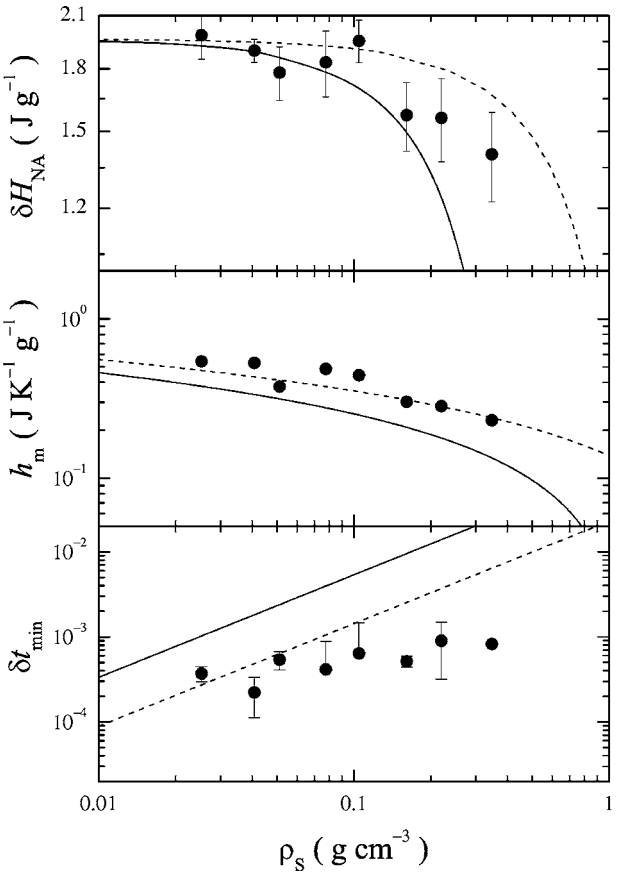

FIG. 4. Scaling analysis of the N-SmA phase transition in $\bar{8}$S5 +sil (solid circles) on log-log scales. Top panel: transition enthalpy δH_{NA}. Middle panel: excess specific-heat maximum $h_m = \Delta C_{NA}^{max}$. Bottom panel: transition rounding in reduced temperature $\delta t_{min} = |t_{min}^-| + |t_{min}^+|$. The bulk scaling predictions are given by Eqs. (9) and (8) where the mean-void length l_0 is used as the cutoff length scale (solid lines) or $3l_0$ (dashed lines).

B. Landau mean-field SmA-SmC scaling analysis

The excess specific heat due to the SmA-SmC phase transition is shown in Fig. 3 for bulk $\bar{8}$S5 and $\bar{8}$S5+sil samples over a temperature range down to $T_{AC} - 4.5$ K. The bulk SmA-SmC transition is well described by an extended Landau theory [23,32] given by

$$\delta C_p(AC) = \begin{cases} 0 & \text{for } T > T_c, \\ A\dfrac{T}{T_c}\left(\dfrac{T_m - T_c}{T_m - T}\right)^{0.5} & \text{for } T < T_c, \end{cases} \tag{10}$$

where A is the $\delta C_p(AC)$ maximum at the transition T_c and T_m is the upper stability limit of the SmC phase. Results from fitting Eq. (10) to the excess specific heat of the SmA-SmC phase transition δC_p for bulk $\bar{8}$S5 and $\bar{8}$S5+sil samples over the temperatures $T < T_{AC}$ are tabulated in Table IV. These results are the average of heating and cooling scan fits. The stability limit of the SmC phase appears to shift upwards from the bulk value by approximately 1.6 K with increasing ρ_S. Although intriguing and indicating a stabilization of the SmC phase with increased ρ_S, given the aging of this particular LC, it is not clear how robust is this result. The fit coefficient A of Eq. (10) appears to smoothly decrease with increasing ρ_S. This is consistent with the behavior of the SmA-SmC transition of 7O.4 in hydrophobic aerosil [13]. The parameter A is also a measure of the tricritical nature of the SmA-SmC transition. A log-log plot shown in Fig. 5 of A versus ρ_S reveals a power-law scaling given by $A \propto \rho_S^{-0.5}$.

IV. DISCUSSION

Results have been presented from a series of high-resolution ac-calorimetric experiments on $\bar{8}$S5+sil dispersions through the N-SmA and SmA-SmC phase transitions as a function of aerosil density. In bulk $\bar{8}$S5, the N-SmA is a nearly clean XY-like transition with $\alpha \lesssim 0$ while the SmA -SmC transition is mean field with a Landau tricritical character. Our bulk measurements are fully consistent with these behaviors. The introduction of QRD in the $\bar{8}$S5+sil system allows for the isolation of random-field, finite-size-like, and

TABLE IV. Summary of the results of fitting Eq. (10) to the excess specific-heat peak δC_p of the Sm*A*-Sm*C* phase transition for $\bar{8}$S5+sil samples. The fit results have been averaged between heating and cooling scans and were done from ~−7 K below T_{AC} to a point slightly below the rounded δC_p peak. The transition temperature T_C and the Sm*C* stability limit T_m are given in kelvins while the coefficient A is given in J K^{-1} g^{-1}. No uncertainty is quoted for T_C as it was fixed to this final value for the last fit iteration.

ρ_S	T_C	T_m	A	χ_ν^2
0	328.957	329.26±0.04	0.108±0.001	1.187
0.025	328.706	330.32±0.38	0.075±0.002	1.208
0.041	329.090	330.61±0.36	0.056±0.002	1.328
0.051	329.010	332.23±0.31	0.049±0.003	1.323
0.078	329.495	330.49±0.25	0.051±0.002	1.258
0.105	329.250	331.08±0.40	0.050±0.010	2.317
0.161	329.390	329.97±0.44	0.025±0.002	1.160
0.220	329.860	331.41±0.19	0.023±0.003	1.206
0.347	329.414	330.37±0.47	0.016±0.002	1.211

elastic strain effects at a pure *XY* and mean-field transition.

The *N*-Sm*A* transition transition temperature does not exhibit a sensitivity to the aerosil (and in fact increases slightly) in stark contrast to that seen in nearly all other LC+sil studies. Although the $\Delta C_p(NA)$ decreases uniformly in size with increasing ρ_S, it remains sharp and is well characterized over the whole range of aerosil concentration. The power-law fits reveal that quasicritical behavior is preserved and that the exponent α_{eff} remains slightly negative and constant for all ρ_S studied. See Fig. 6. The systematic decrease of the coefficients $A^{\pm}$ but nearly constant ratio A^+/A^- is a reflection of the uniform decrease in the size of $\Delta C_p(NA)$ (as well as δH_{NA}). This analysis is consistent with the view that the aerosil gel effectively increases the nematic range. That is, the nematic susceptibility decreases with increasing ρ_S and this is reflected in a substantial change in the pseudocritical properties for cyanobiphenyl-aerosil systems. For $\bar{8}$S5+sil where the bulk material already has a long nematic range, little change is observed.

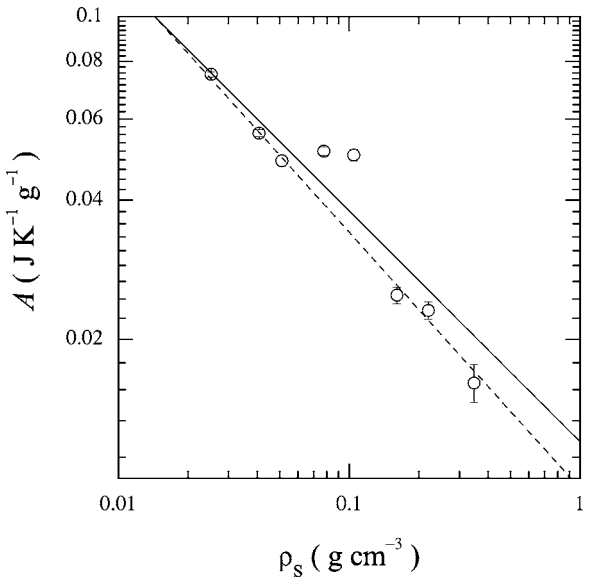

FIG. 5. Scaling plot of A (δC_p at $T=T_{AC}$), obtain from fitting the excess specific heat of the Sm*A*-Sm*C* phase transition to Eq. (10), against ρ_S. The solid line has a slope of −0.5 while the dashed line a slope of −0.56.

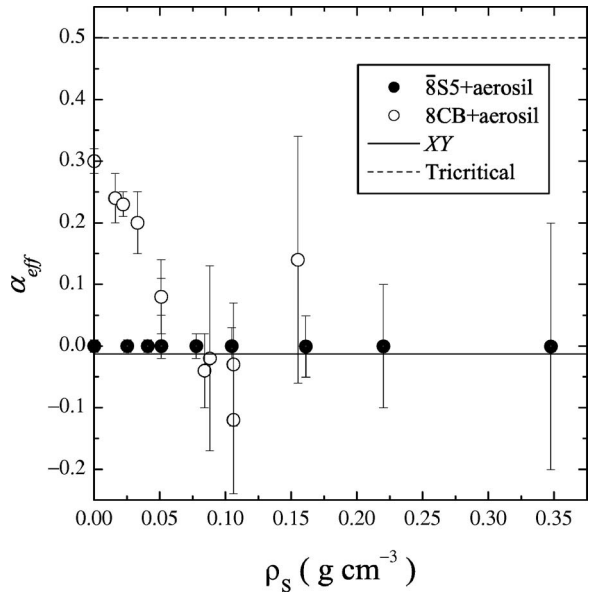

FIG. 6. Comparison of effective specific-heat critical exponent α_{eff} obtained from fitting Eq. (6) to the *N*-Sm*A* phase transition data for $\bar{8}$S5+sil (solid circles) and 8CB+aerosil (open circles) samples.

Because of the good-quality power-law fits available in this study, a detailed scaling analysis was performed and compared to the heat-capacity maximum $h_m=\Delta C_p^{max}(NA)$, transition enthalpy δH_{NA}, and transition temperature rounding $\delta T^*/T^*$ of the *N*-Sm*A* phase transition. This analysis uses the bulk parameters and an adjustable cutoff length scale ξ_M and found excellent agreement for h_m using $\xi_M(\bar{8}\text{S5+sil})=3l_0$ but this does not completely describe the behavior of δH_{NA} nor $\delta T^*/T^*$, especially for $\rho_S>0.1$. Interestingly, when this scaling analysis is applied to the 8CB+sil and 8OCB+sil systems, equally good modeling of h_m is obtained for $\xi_M(8\text{CB+sil})=l_0$ and $\xi_M(8\text{OCB+sil})=1.5l_0$. It is surprising that such excellent agreement is obtained over the whole range of ρ_S explored for these three LC's despite the apparent violation of the classic expectation of finite-size scaling (that is, the truncation of the bulk ΔC_p behavior at the cutoff length scale). Also, the smectic correlation lengths measured for these systems are much larger than this cutoff length scale [33]. This makes the geometric interpretation of the cutoff length puzzling but ultimately connected to the strength of the disorder.

For the mean-field Sm*A*-Sm*C* phase transition, the transition temperature also exhibits very weak sensitivity to the presence of aerosil (even increasing slightly rather than decreasing). This is also in stark contrast to that seen for the Sm*A*-Sm*C* transition in 7O.4+sil and $\bar{8}$S5 in aerogel [27] as well as the Sm*A*-Sm*C** transition of CE8+sil. The heat ca-

pacity associated with the Sm*A*-Sm*C* transition in $\bar{8}$S5+sil presented in this work exhibits a systematic evolution from a Landau tricritical peak to a simple mean-field step with very little smearing observed for $T > T_{AC}$, and then only at the highest ρ_S. Good-quality fits were made using an extended Landau form that found the upper stability temperature increasing with ρ_S, consistent with the shift of the observed transition. In addition, the coefficient A, representing the heat-capacity maximum at the Sm*A*-Sm*C* transition, exhibits a scaling with the aerosil conjugate density as $A \propto \rho_S^{-0.5}$; see Fig. 5. It is clear that this transition, while evolving in a systematic fashion, remains mean field over the entire range of ρ_S studied. This may be a reflection of the Sm*A*-Sm*C* transition behaving as if it were at its upper critical dimension moderating the effect of the QRD produced by the aerosil gel.

In this study of $\bar{8}$S5+sil, it appears that the random-field QRD of the aerosil gel plays a relatively weak role at the *N*-Sm*A* transition (due to the nonpolar molecules and the long nematic range) and also at the Sm*A*-Sm*C* transition (due to either its proximity to its upper critical dimension or that the QRD does not couple linearly to the Sm*C* order parameter and so does not provide a random-field interaction). It is clear that a special length scale is present with $\xi_M > l_0$ but it does not appear to play a leading role for the Sm*A*-Sm*C* transition. How, then, does one understand the evolution of this transition with increasing QRD of aerosil and in light of the other LC+sil and LC+aerogel results? One possibility is that the aerosil gel, due to its flexibility, is closer to thermodynamic equilibrium with the host LC and so causes the LC+sil to behave as a stiffer LC as well as provide QRD. The aerosil gel has been shown to exhibit dynamics coupled to the host liquid crystal [34], and recent work has followed its quenching as aerosil density increases [35,36]. This increase in the effective microscopic elastic stiffness of the LC would be similar to the engineered stiffening of polymer composite materials. A consequence of the stiffening of the nematic phase in LC+sil systems has already been discussed previously [1,14,17,33] in terms of the decrease in the nematic susceptibility with increasing ρ_S to explain the crossover from tricritical to *XY* behavior for the *N*-Sm*A* transition. The present view is to extend this concept to the general stiffening of the LC within the LC+sil.

In the case of the Sm*A*-Sm*C* transition the quenched disorder is also changing the character of the transition. With increasing aerosil density, the peak at the transition is being suppressed in favor of a steplike behavior. This indicates that the transition is being driven away from tricriticality toward mean-field character alone. The proximity to tricriticality is controlled by the layer compression elastic constant B in the modified fourth-order free-energy coefficient $b = b_0 - 2\lambda^2/B$, where b_0 is the original value of this coefficient and λ is the strength of the coupling between the tilt angle and the layer compression [6]. The mean-field phase transition behavior and the decreasing size of the step in the heat capacity are indicative of a hardening of the layer compression elastic constant B.

This effect would serve to explain the evolution of the Sm*A*-Sm*C* transition from Landau tricritical to step in terms of a stiffening of the smectic layer compression modulus B and account for the general stability of the transition temperatures. Note that for $\bar{8}$S5, the nematic and smectic phases are almost fully decoupled in the bulk while there remains significant coupling in the 8CB and 8OCB LC's. It is the latter two LC's that exhibit the strong nonmonotonic transition temperature shifts downward with ρ_S and so may be reflecting QRD effects at the *I*-*N* transition [37]. It would be expected that twisted (or chiral) phases would be more disordered and smeared due to this general LC stiffening as seen in a recent Sm*A*-SmC^* in aerosil study [5]. Also, if the silica gel is too rigid, then this LC stiffening effect is supplanted by the strong quenched disorder as seen in LC in aerogel and in high-density aerosil gel.

Finally, there seems to be an apparent inconsistency between the experimental results of the x-ray study [10] and this calorimetry study on $\bar{8}$S5+sil. In the x-ray work, it is clear that the temperature dependence of the tilt angle of the Sm*C* phase is insensitive to ρ_S, strongly suggesting that the order-parameter ψ for the Sm*C* phase remains unchanged from bulk for all $\bar{8}$S5+sil samples. However, if the system remains mean field, then the relationship $C_p \propto \partial\psi^2/\partial T$ should hold. In this case, the dramatic variation of $\delta C_p(AC)$ with ρ_S suggests that the Sm*C* order-parameter should be strongly ρ_S dependent. Comparison of the δC_p data in Fig. 3 (one data point every 0.1 K) and the tilt angle data in Fig. 6 in Ref. [10] (one data point every $\approx$1 K) suggests that the situation is more ambiguous. A suppression of the tricritical character may be consistent with the more sparse x-ray data (see note [21] in Ref. [10]).

Clearly, there is an important need for theoretical efforts at understanding quenched random disorder on the Sm*A*-Sm*C* transition. The beginnings of such a theory, although for the anisotropic aerogel-disordered Sm*A*-Sm*C* transition [38], are emerging but much is left to be done. A coherent framework must account for the apparent connection with elasticity of both the host material and the disorder-inducing gel. It must also provide for an interpretation of the cutoff length scale that seems to play an important role for the *N*-Sm*A* as well as the observed scaling of the $\Delta C_p(AC)$ peak with ρ_S. Additional x-ray and calorimetric experimental work with anisotropically aligned Sm*A*-Sm*C* as well as Sm*A*-SmC^* in aerosil gel systems is also needed and would provide important data as to the role the polar nature of the LC and the local aerosil-LC interaction.

ACKNOWLEDGMENTS

The authors wish to thank N. A. Clark, C. W. Garland, R. Leheny, and T. Bellini for many helpful and useful discussions. P.S.C. and R.J.B. wish to thank the Natural Science and Engineering Research Council of Canada while staying in Toronto. The funding in Edinburgh was provided by the EPSRC (Grant No. GR/S10377/01). The work at WPI was supported by the NSF under NSF-CAREER Award No. DMR-0092786.

[1] G. S. Iannacchione, Fluid Phase Equilib. **222/223**, 177 (2004), and references cited therein, especially T. Bellini, L. Radzihovsky, J. Toner, and N. A. Clark, Science, **294**, 1074 (2001).
[2] J. D. Reppy, J. Low Temp. Phys. **87**, 205 (1992).
[3] M. Chan, N. Mulders, and J. Reppy, Phys. Today **49**, 30 (1996), and references therein.
[4] R. J. Birgeneau, J. Magn. Magn. Mater. **177–181**, 1 (1998).
[5] G. Cordoyiannis, G. Nounesis, V. Bobnar, S. Kralj, and Z. Kutnjak, Phys. Rev. Lett. **94**, 027801 (2005).
[6] P. G. de Gennes and J. Prost, *The Physics of Liquid Crystals*, 2nd ed. (Clarendon Press, Oxford, England, 1993).
[7] S. Park, R. L. Leheny, R. J. Birgeneau, J.-L. Gallani, C. W. Garland, and G. S. Iannacchione, Phys. Rev. E **65**, 050703(R) (2002).
[8] R. L. Leheny, S. Park, R. J. Birgeneau, J. L. Gallani, C. W. Garland, and G. S. Iannacchione, Phys. Rev. E **67**, 011708 (2003).
[9] P. S. Clegg, C. Stock, R. J. Birgeneau, C. W. Garland, A. Roshi, and G. S. Iannacchione, Phys. Rev. E **67**, 021703 (2003).
[10] P. S. Clegg, R. J. Birgeneau, S. Park, C. W. Garland, G. S. Iannacchione, R. L. Leheny, and M. E. Neubert, Phys. Rev. E **68**, 031706 (2003).
[11] B. Zhou, G. S. Iannacchione, C. W. Garland, and T. Bellini, Phys. Rev. E **55**, 2962 (1997).
[12] H. Haga and C. W. Garland, Liq. Cryst. **23**, 645 (1997).
[13] H. Haga and C. W. Garland, Phys. Rev. E **56**, 3044 (1997).
[14] G. S. Iannacchione, C. W. Garland, J. T. Mang, and T. P. Rieker, Phys. Rev. E **58**, 5966 (1998).
[15] M. Marinelli, A. K. Ghosh, and F. Mercuri, Phys. Rev. E **63**, 061713 (2001).
[16] D. Liang, M. A. Borthwick, and R. L. Leheny, J. Phys.: Condens. Matter **16**, S1989 (2004).
[17] G. S. Iannacchione, S. Park, C. W. Garland, R. J. Birgeneau, and R. L. Leheny, Phys. Rev. E **67**, 011709 (2003).
[18] A. Aharony, Y. Imry, and S.-K. Ma, Phys. Rev. Lett. **37**, 1364 (1976).
[19] A. P. Young, J. Phys. C **10**, L257 (1977).
[20] B. Zhou, G. S. Iannacchione, and C. W. Garland, Liq. Cryst. **22**, 335 (1997).
[21] H. Haga and C. W. Garland, Liq. Cryst. **22**, 275 (1997).
[22] T. Chan, C. C. Bahr, G. Heppke, and C. W. Garland, Liq. Cryst. **13**, 667 (1993).
[23] C. A. Schantz and D. L. Johnson, Phys. Rev. A **17**, 1504 (1978).
[24] C. R. Safinya, Ph.D. thesis, Massachusetts Institute of Technology, Cambridge, MA, 1981.
[25] Degussa Corp., Silica Division, 65 Challenger Road, Ridgefield Park, NJ 07660. Technical data is given in the Degussa booklet AEROSILS.
[26] H. Yao and C. W. Garland, Rev. Sci. Instrum. **69**, 172 (1998).
[27] G. S. Iannacchione, S. Qian, D. Finotello, and F. M. Aliev, Phys. Rev. E **56**, 554 (1997).
[28] A. Roshi, G. S. Iannacchione, P. S. Clegg, and R. J. Birgeneau, Phys. Rev. E **69**, 031703 (2004).
[29] C. W. Garland and G. Nounesis, Phys. Rev. E **49**, 2964 (1994).
[30] The reduced chi-squared parameter

$$\chi_\nu^2 = \frac{1}{\nu}\chi^2 = \frac{1}{\nu}\sum \frac{[y_i - f(x_i)]^2}{\sigma_i^2},$$

where $\nu = N - n$ is the degrees of freedom fitting N data with n parameters in a model $f(x_i)$, is the mean-sqaured deviations normalized to measurement errors σ_i in y_i.
[31] M. Marinelli, F. Mercuri, U. Zammit, and F. Scudieri, Phys. Rev. E **53**, 701 (1996).
[32] M. Meichle and C. W. Garland, Phys. Rev. A **27**, 2624 (1983).
[33] P. S. Clegg, Acta Crystallogr., Sect. A: Found. Crystallogr. **61**, 112 (2005).
[34] C. Retsch, I. McNulty, and G. S. Iannacchione, Phys. Rev. E **65**, 032701 (2002).
[35] R. Bandyopadhyay, D. Liang, R. H. Colby, J. L. Harden, and R. L. Leheny, Phys. Rev. Lett. **94**, 107801 (2005).
[36] A. Roshi, S. Barjami, G. S. Iannacchione, I. McNulty, and D. Patterson (unpublished).
[37] M. Caggioni, A. Roshi, S. Barjami, F. Mantegazza, G. S. Iannacchione, and T. Bellini, Phys. Rev. Lett. **93**, 127801 (2004).
[38] L. Chen and J. Toner, Phys. Rev. Lett. **94**, 137803 (2005).